

Chemometric Study of the Fluorescence of Dental Calculus by Trilinear Decomposition

MARCIA M. C. FERREIRA,* MARY LOU BRANDES, INÊS M. C. FERREIRA, KARL S. BOOKSH,† WILLIAM C. DOLOWY, MARTIN GOUTERMAN, and BRUCE R. KOWALSKI‡

Center for Process Analytical Chemistry and Department of Chemistry, University of Washington, BG-10, Seattle, Washington 98195 (M.M.C.F., M.L.B., I.M.C.F., K.S.B., M.G., B.R.K.); and Animal Care Hospital of Mercer Island, 2705 76th S.E., Mercer Island, Washington 98040 (W.C.D.)

Chemometric techniques have been applied to the unresolved second-order porphyrinic emission-excitation fluorescent spectra of several animal dental calculus deposits dissolved in HCl. A singular value decomposition (SVD) procedure was used for preliminary indication of the number of fluorescent species present in the samples. The trilinear decomposition (TLD) method was applied to resolve component spectra, resulting in three porphyrinic spectral profiles for both canines and felines.

Index Headings: Trilinear decomposition; Curve resolution; Total luminescence spectra; Animal dental calculus; Porphyrins.

INTRODUCTION

In the chemometrics literature, several papers have appeared¹⁻⁷ that deal with so-called second- and third-order data analysis methods. Such data are generated by hyphenated instruments which have become commonplace in analytical laboratories.⁸ Total luminescence spectra,⁹ for example, are generated by a hyphenated technique that gives two-dimensional arrays of data for each sample, where each row is an emission spectrum and each column an excitation scan. However, while theoretical research developing optimal methods of data analysis for hyphenated techniques progresses nicely, there have been very few applications.^{10,11} This paper presents an application of chemometric resolution to the total luminescence spectra of calculus from domestic animals.

Veterinary dentists are interested in dental calculus on animal teeth,^{12,13} which can lead to periodontal disease. Red fluorescence has been observed in animals when dental calculus is irradiated with ultraviolet light, and preliminary analysis suggests that dog (canine) calculus contains at least three porphyrin compounds,¹⁴ although the spectra could not be fully resolved. The analyzability of dental calculus samples is limited by the small sample size. Although the calculus samples are large enough to allow one to obtain total luminescence spectra, the samples are too small to allow one to perform feasible quantitative or qualitative chromatographic separation in order to resolve the component porphyrins. However, spectral resolution performed to count and separate porphy-

rins can be accomplished mathematically, instead of physically.

The analysis in this paper shows that mathematical resolution of incompletely resolved second-order data is a viable alternative when chromatographic resolution is impractical because of constraints, such as sample size or cost. The trilinear decomposition (TLD) algorithm⁷ is employed to analyze the second-order spectra of four cat (feline) and three canine calculus samples. Stable, physically meaningful estimates of three characteristic porphyrin excitation and emission profiles are obtained in spite of slight nonlinear deviations from the rigorous model assumed by the TLD algorithm. It is shown in this paper that TLD can readily be used to distinguish factors that describe particular chemical information from factors that describe nonlinearities.

THEORY

Rank annihilation factor analysis (RAFA), introduced by Ho et al.¹ and later reformulated by Lorber^{2,15} as an eigenvalue problem, has proven to be a useful tool for the analysis of two-dimensional data arrays. Here, the data matrix for one sample, **R**, contains unique information in the row space and the column space. These kinds of data are produced by second-order instruments which are, in general, a combination of two first-order instruments where one instrument modulates the response of the other. Among these hyphenated instruments are liquid chromatography/ultraviolet (LC/UV), gas chromatography/mass spectroscopy (GC/MS), and emission-excitation spectrofluorimeters, all of which are classified as bilinear since the response matrix for a pure component has rank one. MS/MS and two-dimensional nuclear magnetic resonance (2D-NMR) are nonbilinear because the rank of the response matrix for a pure component is greater than one.^{16,17}

A noniterative, generalized rank annihilation method (GRAM)³ is readily applied to the simultaneous analysis of two second-order samples. With GRAM, it is possible to obtain a unique decomposition of two bilinear response matrices which gives estimates of the pure profiles (qualitative results) present in both samples and also the concentration ratios of the pure components in both samples (quantitative results). Wilson et al.¹⁸ and Li et al.¹⁹ have since improved and extended the algorithm for GRAM to make it more robust and to implement similarity transformations to aid in the interpretation of the estimated profiles.

Received 31 October 1994; accepted 28 April 1995.

* On leave from Universidade Estadual de Campinas, Campinas, SP Brazil 13081-970.

† Present address: University of South Carolina, 700 S. Main St., Columbia, SC 29208.

‡ Author to whom correspondence should be sent.

The scenario becomes more complex when several samples are to be simultaneously analyzed. In this case, the experimental data set can be structured into a three-dimensional array, \mathbf{R} , by stacking K two-dimensional data matrices, $\mathbf{R}_1, \dots, \mathbf{R}_K$, obtained from the respective samples. Sanchez and Kowalski⁷ proposed a method called trilinear decomposition to deal with these three-way data matrices, for the case where the response behaves linearly in each of the three modes, as shown below.¹ TLD performs a triadic decomposition on the data set \mathbf{R} . With total luminescence spectra, the instrument response at the i th emitting wavelength for the j th excitation wavelength of the k th sample is modeled by

$$R_{ijk} = \sum_{n=1}^N X_{in} Y_{jn} Z_{kn} \quad (1)$$

where N is the number of factors, or the rank, in the model.²⁰ If each \mathbf{R}_k is bilinear and there is no collinearity among the excitation profiles, the emission profiles, or the concentrations, the columns of the \mathbf{X} , \mathbf{Y} , and \mathbf{Z} matrices correspond, respectively, to true excitation, true emission, and true concentration profiles of the N species in \mathbf{R} . When only the ratio of concentrations, \mathbf{Z} , can be estimated rather than the absolute values, the resulting spectral profiles, \mathbf{X} and \mathbf{Y} , must be scaled. Normalization by the Euclidean norm specifies one curve which represents the qualitative shape of the spectrum. If the main goal is curve resolution, as in this paper, this lack of quantitative information is not a problem.²¹

According to the TLD model, the rank of each pure component matrix is unitary, in the absence of noise, so that the number of pure components is equal to the total rank. But in the presence of spectral nonlinearities and noise, small departures from a complete trilinear structure are common and the rank of each pure component is no longer exactly one. To correct for nonlinearities introduced by unavoidable experimental error, one adds additional factors. However, the mathematical model alone cannot give sufficient criteria to determine whether a factor is real or it results from a nonlinearity. By carefully studying plots of the estimated profiles in the X and Y mode from a chemical perspective, it is possible to determine whether a minor factor describes a nonlinear effect or a particularly dilute chemical species.⁴

EXPERIMENTAL

Samples of calculus, removed from the teeth of canines and felines, were dissolved in 27% HCl and gravity-filtered prior to spectral analysis.²² The fluorescence was studied on a Perkin-Elmer LS50 luminescence spectrophotometer with a xenon flash tube as the excitation source and 1-cm² quartz cuvette as the sample cell. The instrument has an excitation and emission monochromator allowing two types of spectra. An excitation spectrum is obtained by scanning the excitation monochromator with the emission monochromator kept at a fixed λ_{detect} , and an emission spectrum is obtained by scanning the emission monochromator with the excitation monochromator kept at a fixed λ_{excite} .

Specimens from three canines and four felines were studied, with 30 emission spectra taken for each sample.

Each emission spectrum ranged from 460 to 750 nm in one-half-nanometer increments and was taken at λ_{excite} wavelengths in 2-nm increments from 392 to 450 nm.

The data matrix \mathbf{R} for each sample was constructed by taking the intensity values R_{ij} for the i th emission wavelength and the j th excitation wavelength, giving it a dimension of 581×30 . The matrices were graphically represented by plotting the intensity values R_{ij} in the z axis, for each (i, j) point in the (x, y) plane. The calculations were performed on a Digital Personal DECstation 5000/25 with the TLD routine⁷ written in MATLAB environment. Computation time for the complete analysis of each TLD model was less than 1 min.

RESULTS

Analysis was performed on the 251×30 truncated matrices, with emission wavelengths from 585 to 710 nm, because visual inspection of the instrument response matrices showed no significant emission from 460 to 585 nm and from 710 to 750 nm. Figure 1 shows three-dimensional and contour plots of the truncated raw data for two of the seven samples, one feline and one canine. The plots for the other samples are similar but differ primarily in the intensity values and slightly in the maximum excitation or emission intensity wavelengths.

The singular value decomposition (SVD) procedure was applied to determine the number of factors needed to model the fluorescing species present in each sample and the total number of fluorescing species present in the data; a significant singular value indicates a major factor, whereas very small singular values are associated with experimental error. Each individual sample is well described by three factors, although the fourth factor, albeit quite small, describes nonrandom variance. This same result is obtained, as shown in Table I, when all the feline sample matrices are juxtaposed either row-wise or column-wise and analyzed as one single matrix. Since each singular value (s) represents a portion of the total variation in the data, the total (cumulative) percent variance of the measured spectra, given by

$$\text{Total \% Variance} = \frac{\sum_{i=1}^N (S_i)^2}{\sum_{i=1}^P (S_i)^2} \times 100, \quad (2)$$

was calculated; the results for the first ten factors are also given in Table I. In Eq. 2, N is the number of factors in the model, and P is the total number of singular values in the system. The four-factor model expresses 99.967% and 99.976% of the total variance for data matrices juxtaposed row-wise and column-wise, respectively. Since measured spectra always contain some noise, it is quite reasonable to assume that the remaining 0.03% is due to those effects. With the application of the same procedure to the combined canine samples, the results showed a slight discrepancy between the column-wise and the row-wise analysis (Table I), suggesting the presence of nonlinearities in the emission mode (X space). With all seven samples in one composite group, the results indicate that the fourth and the fifth factors, although small, also describe nonrandom variance. Therefore, it is concluded

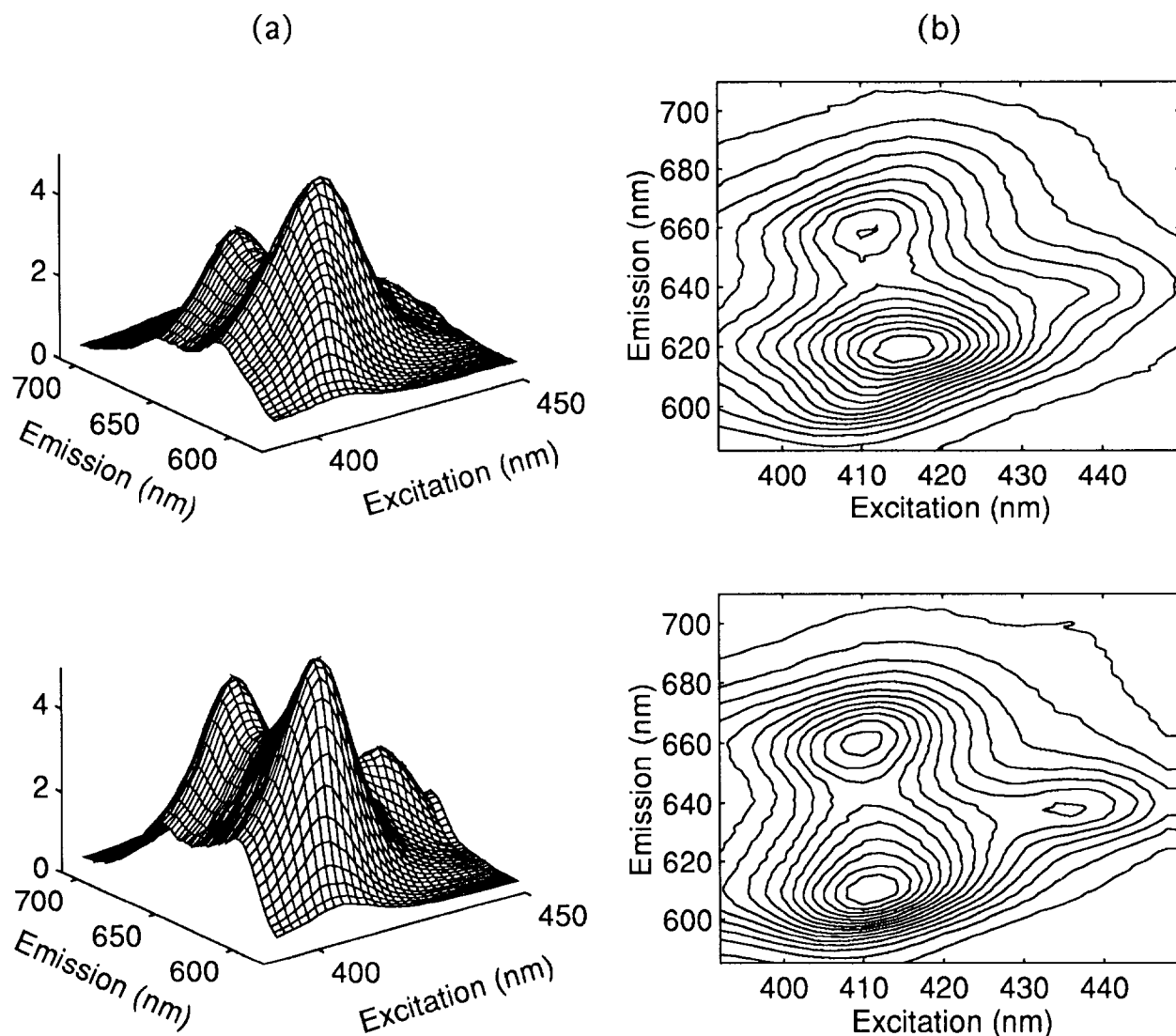


FIG. 1. Total luminescent spectral surface of the truncated raw data for feline (upper) and canine samples (lower) (a), and the respective contour plots (b).

that all seven samples contain fluorescing species in common. However, the total number of species present, as well as the number of fluorescent species in common, could not be determined by the SVD analysis; therefore, the TLD method was applied with an increasing number of factors.

Feline Samples. With the application of the TLD method to the combined feline samples ($\text{dim } \mathbf{R} = 251 \times 30 \times 4$), two luminescent profiles can be resolved with a two-factor model. The first type, designated porphyrin I, has excitation maximum at 410 nm and emission maxima at 604.5 and 659 nm, and the second type, designated porphyrin II, has excitation maximum at 419 nm and emission maxima at 621 and 672 nm. The spectral profiles from the two-factor model are shown in Fig. 2 and correspond to the expected appearance of porphyrinic emission and excitation spectra. The estimated emission profiles are positive and have maxima in the wavelength regions expected for protonated porphyrins. The excitation profiles are non-negative and, in general, unimodal and are indicative of porphyrinic Soret bands.²³ Although

this two-factor model seems quite adequate at describing the data, the results from Table I indicate that the third and fourth factors contain nonrandom variance. It is of interest to determine whether the lesser factors describe additional chemical species or nonlinearities in the data set.

Looking at the truncated raw data (Fig. 1), especially the contour plot, it can be seen that there exists a shoulder at the excitation wavelength between 430 and 450 nm. This observation indicates that a third profile, porphyrin III, with a small molar extinction coefficient²³ and/or in relatively small concentration, can be resolved. Overall, the quality of the estimated spectra from the three-factor model is good, as shown in Fig. 3. The plots show a very reasonable spectra estimate for porphyrin III, which has an excitation band at 435 nm and maximum emission at 637 nm. Indeed, the \mathbf{Z} matrix(1), which in this case indicates the total relative luminescence, confirms that the spectral intensity of porphyrin III in all four feline samples is small in comparison to the results for the other two. Although the decomposition produced a good esti-

TABLE I. Singular values and cumulative percent variance^a of the measured spectra for the first ten factors.

Data matrices row-wise juxtaposed.					
Felines		Canines		All samples	
Singular values	Total % variance	Singular values	Total % variance	Singular values	Total % variance
309.169	97.852	333.060	92.074	450.507	93.030
38.424	99.363	93.845	99.384	112.415	98.823
23.346	99.921	23.887	99.858	46.629	99.819
6.719	99.967	10.452	99.948	15.290	99.926
3.811	99.982	6.702	99.986	9.815	99.971
2.940	99.991	2.480	99.991	5.825	99.986
1.537	99.993	2.070	99.994	3.679	99.992
0.655	99.994	0.932	99.995	1.722	99.994
0.619	99.994	0.756	99.996	1.138	99.994
0.616	99.995	0.633	99.996	1.049	99.995

Data matrices column-wise juxtaposed.					
Felines		Canines		All samples	
Singular values	Total % variance	Singular values	Total % variance	Singular values	Total % variance
308.966	97.723	330.148	90.471	446.337	91.316
40.244	99.381	103.958	99.442	129.463	98.998
22.988	99.922	23.496	99.900	43.970	99.885
7.285	99.976	8.876	99.965	11.015	99.940
3.400	99.988	5.436	99.990	9.955	99.986
2.158	99.993	1.866	99.993	3.234	99.990
1.066	99.994	1.610	99.995	2.618	99.994
0.790	99.995	0.954	99.995	1.297	99.994
0.725	99.995	0.705	99.996	1.209	99.995
0.689	99.996	0.658	99.996	0.986	99.995

^a Calculated according to Eq. 2.

mated emission profile, the estimated excitation spectrum of porphyrin III is not unimodal, as expected (Fig. 3). There is a minimum at 412 nm which is located within the region where the excitation peaks for the other profiles highly overlap. The excitation and emission profiles for porphyrin II show a slight negative region above 437 nm and 590–596 nm, but these correspond only to 2% and 0.2% of the main peaks, respectively.

A fourth factor in the model supports the conclusion that the third factor describes an additional porphyrinic profile. The four-factor model yields three excitation profiles (Fig. 4) where only the excitation profile of porphyrin III is not unimodal and has a deviation into the negative region. This negative region is equivalent to less than 9% of the main peak. With the introduction of the fourth factor, the results show that the overall peak shape of porphyrin III in the excitation mode has improved in the region of low overlap, to reflect a more porphyrinic shape. The halfwidth has dropped from 24 nm in the three-factor model to 20 nm in this model. The sinusoidal shape shown in Fig. 3 between 396 and 416 nm has disappeared, although the minimum coinciding with the largest overlap between porphyrin I and II is still present but less pronounced. The negative intensities above 437 nm for porphyrin II (Fig. 3) have also been corrected, but, on the other hand, the excitation profile for porphyrin I is slightly negative in the region 430 to 446 nm (only 1% of the main peak). The emission profiles, shown in Fig. 4, were also affected by the addition of the fourth factor into the model. The emission peak of porphyrin III is narrower in the region of less overlap, with halfwidth of 20 nm compared to 37 nm in the three-factor model, and

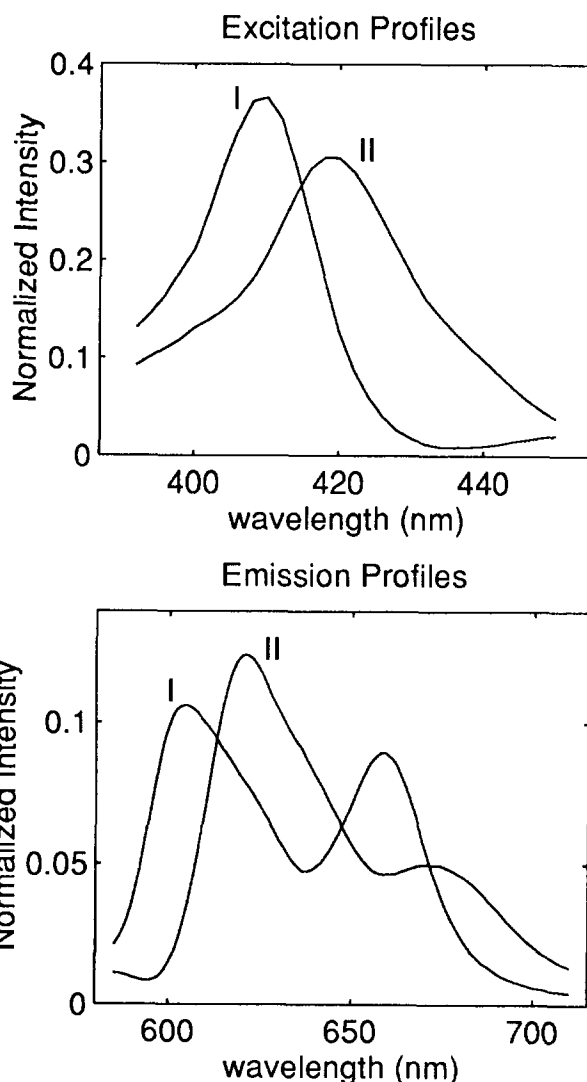


FIG. 2. Estimated excitation and emission profiles from four feline calculus excitation–emission fluorescence spectra when decomposed by a two-factor TLD model. The spectral profiles are normalized to unit length (see text).

it is apparent in this model that porphyrin III has a second broad, weak peak at 701 nm. The negative intensities for porphyrin II have been corrected, but the estimated emission profile for porphyrin III is in the negative region from 590 to 625 nm. Although this negative region is equivalent to 38% of the main peak area, it occurs where the intensity would be expected to have very small values in comparison to the intensities of porphyrin I and II. Also, the addition of this fourth factor introduces some random noise into the model. The fourth factor describes nonlinearities that affect the shape of the profiles. From the chemical perspective, the estimated excitation profile is not porphyrinic. However, the respective emission profile is chemically meaningful since it is similar in shape to the profile of porphyrin I but shifted to the blue region of the spectra.

Table II shows a summary of the maximum intensity locations for these three profiles. Comparing the three- and four-factor models, it can be seen that the excitation and emission peaks for the four-factor model show a slight

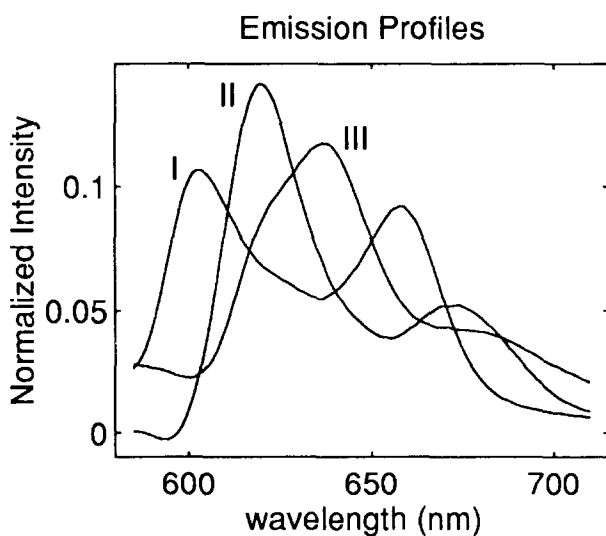
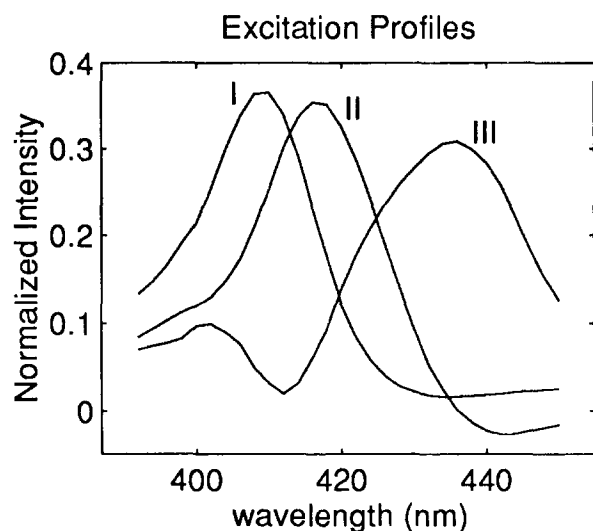


FIG. 3. Estimated excitation and emission profiles from four feline calculus excitation-emission fluorescence spectra when decomposed by a three-factor TLD model. The spectral profiles are normalized to unit length.

red shift in comparison to results for the three-factor model. In summary, it is concluded that in the feline data, in spite of spectral nonlinearities, there are three porphyrinic profiles that can be resolved.

Canine Samples. According to the TLD method, decomposition of the three combined canine samples provides reasonable spectral profiles for two porphyrin types. The first has an excitation peak indicative of a Soret band at 411 nm and emission maxima at 611 and 660.5 nm. The second has excitation and emission peaks at 436 and 637.5 nm, respectively. The emission and excitation profiles obtained with the two-factor model are shown in Fig. 5. It is interesting to note that the first shows fluorescent peaks in the same region as porphyrin I from the feline samples, and the second has fluorescent peaks in the same region as porphyrin III from the felines; therefore they are referred to as porphyrin I and porphyrin III, respectively. The emission profile for porphyrin III (Fig. 5) is not unimodal, and it has a second broad and very weak peak at 682 nm, consistent with the contour plot of trun-

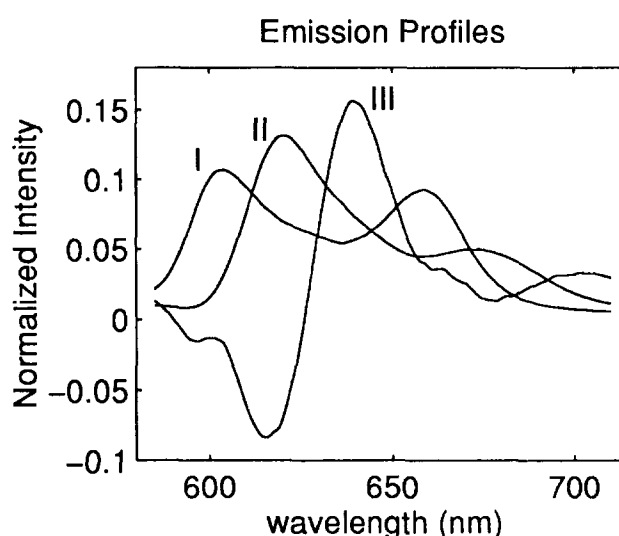
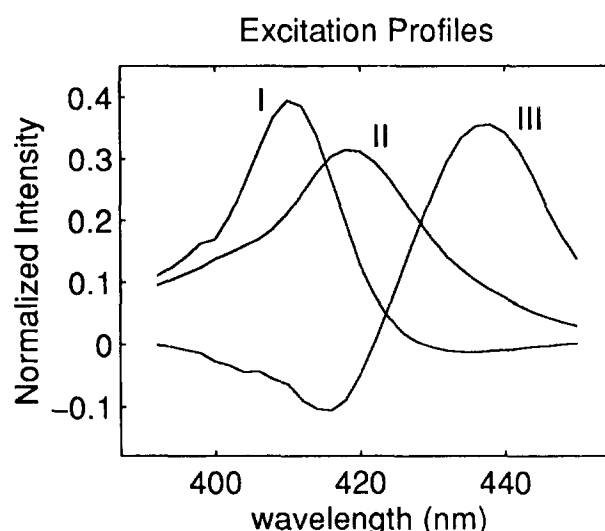


FIG. 4. Estimated excitation and emission profiles from four feline calculus excitation-emission fluorescence spectra when decomposed by a four-factor TLD model. The spectral profiles are normalized to unit length.

cated raw data in Fig. 1b. The emission profile for the corresponding species in the feline samples predicted a second peak in the four-factor model at 701 nm, even though the signal was too small to be visible in the contour plot.

If we look at the truncated raw data for the canine, especially at the contour plot (Fig. 1b), a third profile with an excitation band at 418 nm is not obvious. However, according to the results in Table I, the third factor expresses nonrandom variance. When a three-factor model is used, it is clear that, as in the feline case, there is a third porphyrinic profile in the canine data (Fig. 6). The *Z* matrix indicates that the total relative luminescence for this compound is small in comparison with the other two. The decomposition clearly resolves three profiles with plausible porphyrinic peak positions. Porphyrin I and III have excitation maxima at 410 and 436 nm, respectively, and emission peaks at 609.5 and 659 nm for porphyrin I and 638 nm for porphyrin III. The excitation peak for the third profile, located at 420 nm, and the

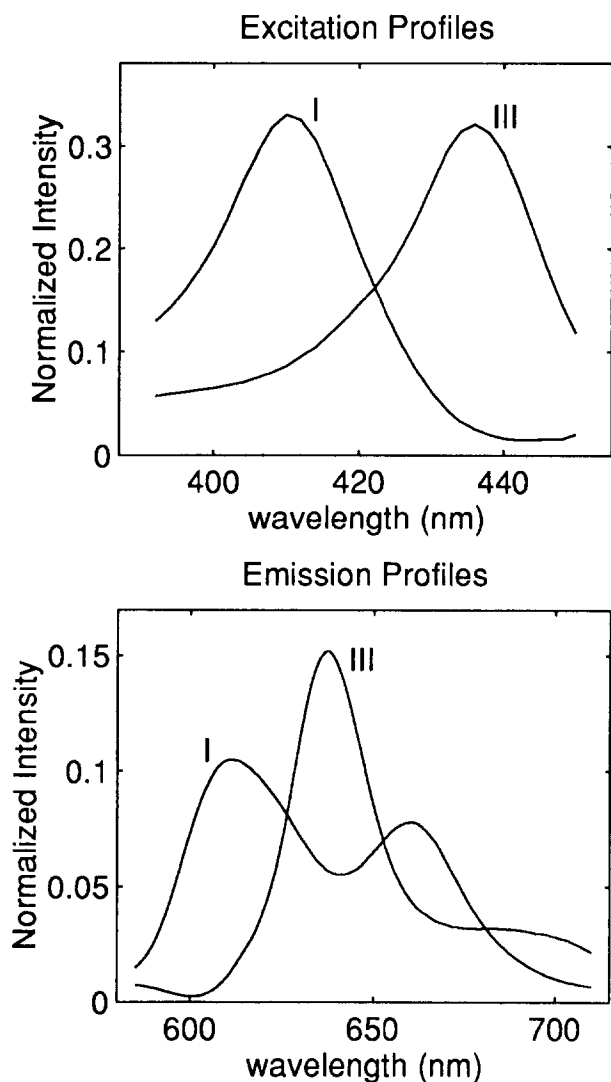


FIG. 5. Estimated excitation and emission profiles from three canine calculus excitation–emission fluorescence spectra when decomposed by a two-factor TLD model. The spectral profiles are normalized to unit length.

emission peaks at 623.5 and 679 nm indicate that this profile may have the same basic structure as porphyrin II from the feline samples, and therefore will be similarly designated.

The excitation profile of porphyrin II is not unimodal and presents two negative regions corresponding to 3% and 10% of the main peak (see Fig. 6). The respective emission profile contains two negative peaks (27% and 16%). This result is not totally surprising since the data do not follow the perfect linear model, and this deviation affects most strongly the porphyrin II, which has low relative spectral intensity and is highly overlapped with porphyrin I. As in the previous case (Fig. 4), the negative intensities in Fig. 6 occur in the region where either the intensities should have small values or the overlap among all three profiles is the highest. According to the SVD/total variance analysis, the fourth factor (and the fifth, when the matrices are row-wise juxtaposed) reveals non-random variance and suggests that the model should be tested with additional factors.

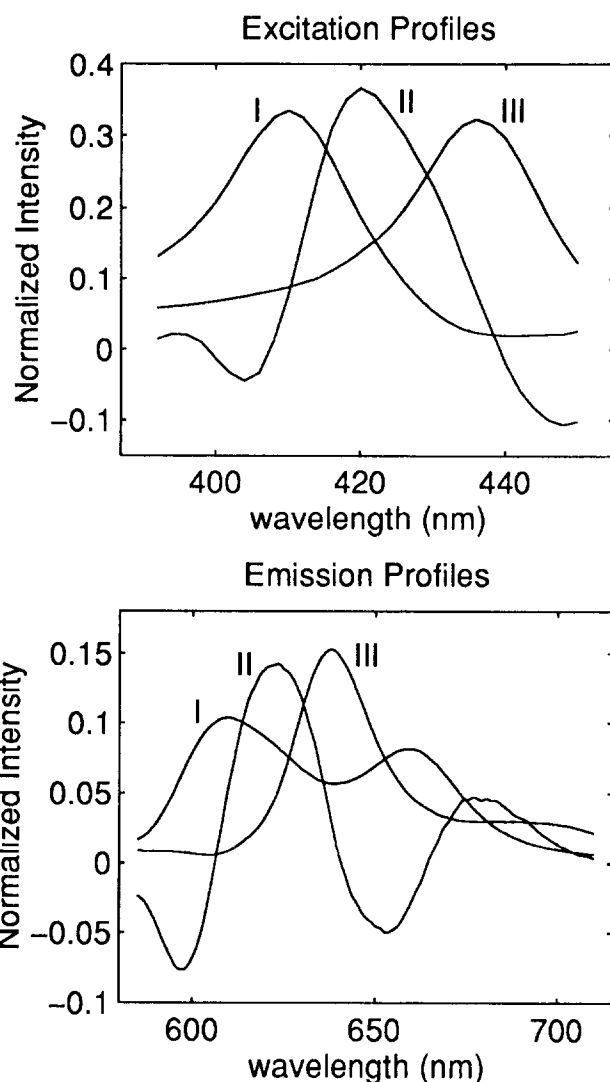


FIG. 6. Estimated excitation and emission profiles from three canine calculus excitation–emission fluorescence spectra when decomposed by a three-factor TLD model. The spectral profiles are normalized to unit length.

Of the four- and five-factor models, the five-factor model yields the most visually appealing spectra. A summary of the results obtained for the four-factor model is in Table III. In this model, the excitation peak for porphyrin II that would be expected in the region of 420 nm has disappeared. Instead, two new profiles have been estimated, one with a large negative region at lower wavelengths and a small positive portion where the peak is anticipated for porphyrin II. This profile does not appear to be chemically meaningful. The other excitation profile is red-shifted relative to porphyrin III.

The spectral profiles for porphyrins I, II, and III, in the five-factor model, are shown in Fig. 7. Three reasonable porphyrinic excitation profiles are estimated. They are all positive, and only the profile for porphyrin II presents a slight deviation from unimodality. The other two profiles, not shown, are not porphyrinic. The emission profiles for porphyrins I and III match reasonably well with the respective profiles from the three-factor model. However, the porphyrin II emission profile is not well modeled;

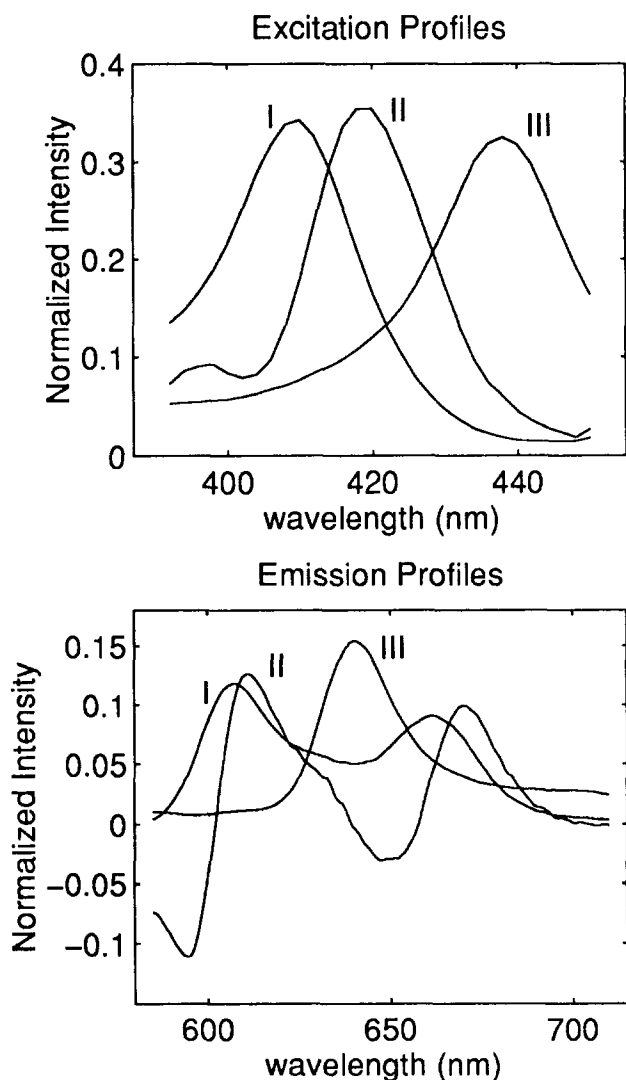


FIG. 7. Estimated excitation and emission profiles from three canine calculus excitation-emission fluorescence spectra when decomposed by a five-factor TLD model. The spectral profiles are normalized to unit length.

besides the presence of a negative region at low wavelengths, it is also very blue shifted (Fig. 7). These results also can be verified in Table III, where the Soret bands and emission peaks for the different models considered

TABLE II. Soret bands and emission peaks for the three porphyrins resolved by TLD method using different models for the feline calculus samples.

Soret bands (in nm to ± 1)	Porphyrin I	Porphyrin II	Porphyrin III
Two-factor model	410	419	—
Three-factor model	409	417	435
Four-factor model	410	418	437
Emission peaks (in nm to ± 0.5)	Porphyrin I	Porphyrin II	Porphyrin III
Two-factor model	604.5	621	—
	659	672 ± 1	—
Three-factor model	602.5	620	637
	658	673	—
Four-factor model	604	620	639
	659	673 ± 1	701 ± 1.5

TABLE III. Soret bands and emission peaks for the three porphyrins resolved by TLD method using different models for the canine calculus samples.

Soret bands (in nm to ± 1)	Porphyrin I	Porphyrin II	Porphyrin III
Two-factor model	411	—	436
Three-factor model	410	420	436
Four-factor model	409	—	434
Five-factor model	409	419	437
Emission peaks (in nm to ± 0.5)	Porphyrin I	Porphyrin II	Porphyrin III
Two-factor model	611	—	637.5
	660.5	—	682 ± 2
Three-factor model	609.5	623 ± 0.75	638
	659 ± 1	679 ± 1.5	—
Four-factor model	613	—	636
	662	—	689 ± 1
Five-factor model	607	611	640.5
	662	670	—

above are presented. The SVD and total percent variance (Table I) for the row-wise juxtaposition suggested the presence of nonlinearities in the emission mode, and that consideration, unfortunately, might have led to the difficulties in completely resolving the spectra. However, it can be concluded that the canine spectra contain three resolvable porphyrinic profiles. The excitation bands from these are the same as those found for the felines with the resolution of the available data, and their emission spectra are similar as well. This observation is a strong indication that porphyrin I, II, and III are also present in canines.

Feline Canine Samples. The decomposition of the canine and feline samples yields very similar porphyrinic profiles. It is expected, therefore, that the trilinear decomposition of the canine and feline samples combined into one data matrix will give a reasonably good deconvolution and that the results will be similar to those obtained for the feline and canine samples when analyzed individually. The profiles for the three-factor model of the combined samples are shown in Fig. 8 with the peak locations shown in Table IV. The excitation profile for porphyrin I is not unimodal, and it has a small negative region. The emission profile also has two small negative regions (0.9% and 1.8% of the peak area).

TABLE IV. Soret bands and emission peaks for the three porphyrins resolved by TLD method when applied to all calculus samples using different models.

Soret bands (in nm to ± 1)	Porphyrin I	Porphyrin II	Porphyrin III
Three-factor model	407	414	436
Four-factor model	407	414	437
Five-factor model	410	417	436
Emission peaks (in nm to ± 0.5)	Porphyrin I	Porphyrin II	Porphyrin III
Three-factor model	602	619	638
	657.5	661 ± 1	—
Four-factor model	601	619	638
	657	665 ± 1	—
Five-factor model	604	620	638
	658.5	670.5	—

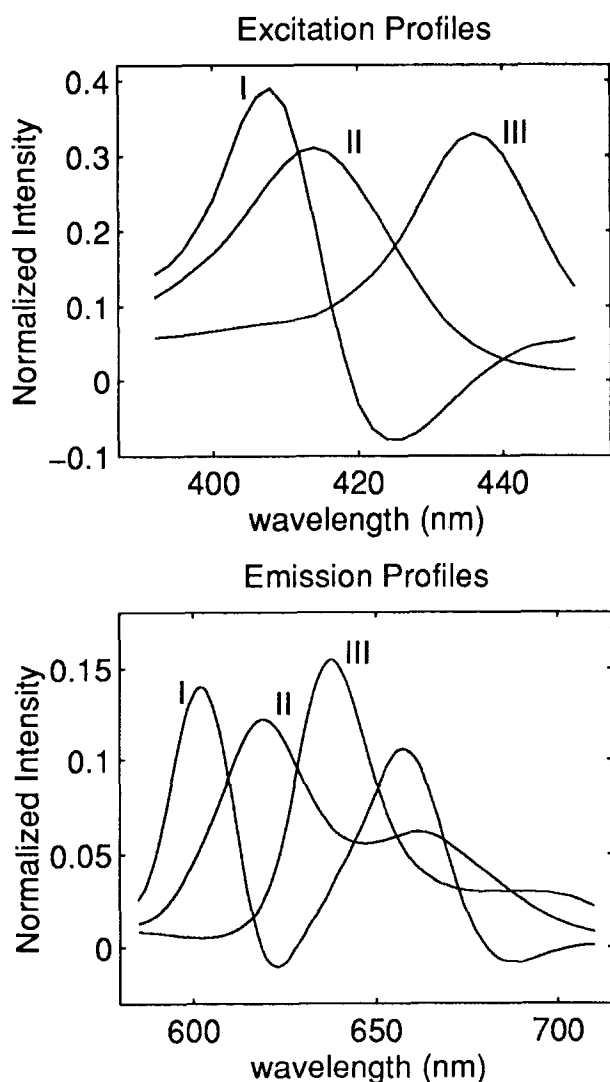


FIG. 8. Estimated excitation and emission profiles from four feline and three canine calculus excitation–emission fluorescence spectra when decomposed by a three-factor TLD model. The spectral profiles are normalized to unit length.

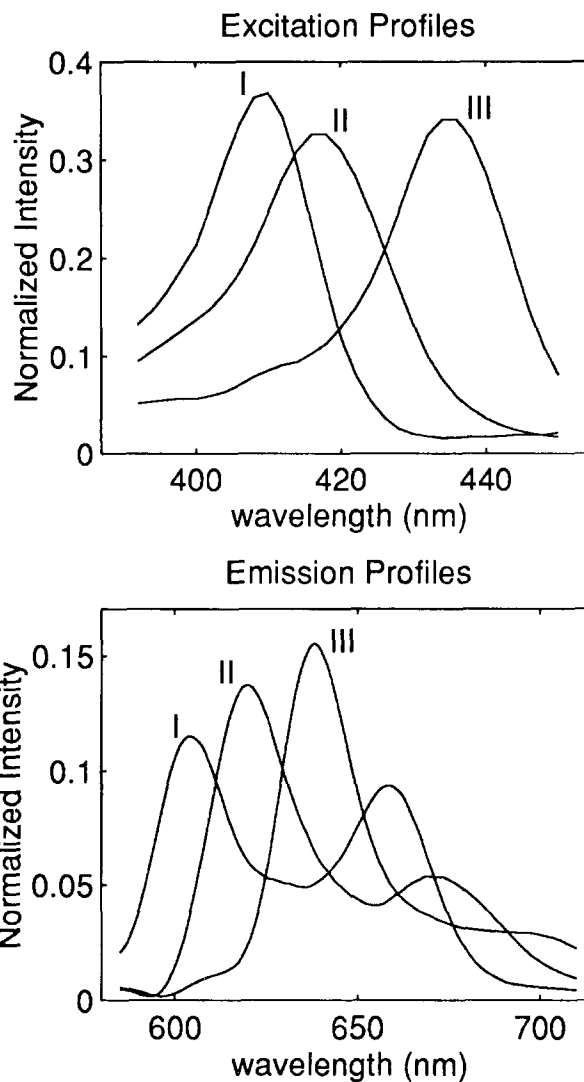


FIG. 9. Estimated excitation and emission profiles from four feline and three canine calculus excitation–emission fluorescence spectra when decomposed by a five-factor TLD model. The spectral profiles are normalized to unit length.

With the introduction of one more factor into the model, the porphyrinic character of porphyrin I is expected to improve because of the significant, although small, fraction of the total variance that it contains. The new factor describes nonlinearities without describing a new porphyrinic profile, but the system as a whole would be expected to be better described. Indeed, the four-factor model corrects those negative regions in both excitation and emission modes, but one excitation profile still does not seem to be perfectly resolved; it is not unimodal, although it is positive. Table IV contains the peak positions for the three resolved profiles.

It is evident from the four-factor model that there are three porphyrinic profiles that can be resolved for the analyzed samples, but the fifth factor still describes non-random variance. When an additional factor is included in the model (Fig. 9), the excitation profiles are unimodal, and the two lesser factors describe only nonlinearities in the data, rather than a new porphyrinic profile. This improvement in the excitation profiles when these two extra

factors are included is evident from the improvement in the shape and peak position of the profiles (Figs. 8 and 9 and Table IV). They are all positive, and their peaks, positioned at 410, 417, and 436 nm, respectively, for porphyrins I through III, are in better agreement with those obtained for felines and canines analyzed individually (Figs. 4, 7, and 9 and Tables II–IV). The emission profiles are all positive and are fairly similar in shape and peak position to those obtained for felines with a four-factor model and canines with the three- or five-factor model.

Considering all the samples together, three fully resolved (i.e., all chemically meaningful and positive) spectra estimates are obtained, corresponding to porphyrins I, II, and III. The excitation peaks are well defined within the 2-nm range that reflects the fixed λ_{excite} intervals. For the felines, the total relative luminescence of porphyrin III is much less than that of I and II, while for the canine samples, porphyrin II has lower total relative luminescence.

CONCLUSION

It is clear from the chemometric analysis above that, even in the presence of nonlinearities, fully resolved estimates of three porphyrinic spectral profiles present in the animal dental calculus can be nicely attained. The estimated excitation and emission profiles have peaks in regions expected for protonated porphyrins. Three porphyrinic profiles in the feline samples can be resolved, and these are similar in shape and peak location to those resolved in the canine samples. Porphyrin I and II are dominant in the felines, while porphyrin I and III are dominant in the canines. The TLD method was shown to be a useful tool in distinguishing the factors which describe chemical information from those that account for deviations of the data set from the ideal linear model.

Each of the profiles we have designated as porphyrin I through III may be estimated spectral profiles of porphyrins from the dental calculus, or they may each originate from a mixture of porphyrins too similar to resolve. However, they can be presumed to have the same central porphyrin²³ structure within each designation, differing only slightly in peripheral function side group (for example, a peripheral side group of acetic acid vs. propionic acid). Porphyrin I and II are more similar than porphyrin I and III or porphyrin II and III from a spectroscopic perspective. This observation most likely reflects a similar central structure in porphyrin I and porphyrin II and a significant difference in the structure of the porphyrin side chains.²⁴ The difference between porphyrin I and porphyrin III and porphyrin II and porphyrin III most likely reflects a different porphyrin nucleus. The resolved spectra suggest that the luminescence comes from a metal-free porphyrin.¹³ These metal-free porphyrins are most likely protoporphyrin derivatives derived from biological porphyrins after the iron has been "stolen" from the heme. Further work to identify the porphyrins in the profiles obtained in this study is planned.

ACKNOWLEDGMENTS

M. M.C.F. is happy to acknowledge the financial support from CNPq (Brazil) and UNICAMP (Brazil), and the scientific environment kindly

provided by the CPAC (UW), where this work was developed. M.L.B. kindly acknowledges funding for her graduate work for the NASA Graduate Student Research Program. K.S.B. is funded by an American Chemical Society–Division of Analytical Chemistry/Dupont Graduate Fellowship.

1. C.-N. Ho, G. D. Christian, and E. R. Davidson, *Anal. Chem.* **50**, 1108 (1978).
2. A. Lorber, *Anal. Chim. Acta* **164**, 293 (1984).
3. E. Sanchez and B. R. Kowalski, *Anal. Chem.* **58**, 496 (1986).
4. J. Öhman, P. Geladi, and S. Wold, *J. Chemo.* **4**, 79 (1990).
5. P. Kroonenberg and J. de Leeuw, *Psychometrika* **45**, 69 (1980).
6. D. S. Burdick, X. M. Tu, L. B. McGown, and D. W. Millican, *J. Chemo.* **4**, 15 (1990).
7. E. Sanchez and B. R. Kowalski, *J. Chemo.* **4**, 29 (1990).
8. T. Hirshfeld, *Anal. Chem.* **52**, 297 A (1980).
9. G. D. Christian, in *Instrumental Analysis* (Allyn and Bacon, Boston, 1986), 2nd ed., pp. 247–275.
10. M. Marchiarullo and R. Ross, *Biochim. Biophys. Acta* **807**, 52 (1985).
11. R. T. Ross, C-H Lee, C. Davis, B. Ezzedine, E. Fayyad, and S. Leugrants, *Biochim. Biophys. Acta* **1056**, 317 (1991).
12. W. C. Dolowy, *J. Am. Veterinary Medical Assn. Lett.* **201**, 530 (1992).
13. W. C. Dolowy, J. D. Parker, M. L. Brandes, and M. Gouterman, *J. Am. Veterinary Medical Assn. Lett.* **206**, 26 (1995).
14. W. C. Dolowy, M. L. Brandes, M. Gouterman, J. D. Parker, and J. Lind, *J. Vet. Dent.*, paper in press.
15. A. Lorber, *Anal. Chem.* **57**, 2397 (1985).
16. E. Sanchez and B. R. Kowalski, *J. Chemo.* **2**, 265 (1988).
17. K. Booksh and B. R. Kowalski, paper submitted to *J. Chemo.* (1994).
18. B. E. Wilson, E. Sanchez, and B. R. Kowalski, *J. Chemo.* **3**, 493 (1989).
19. S. Li, C. Hamilton, and P. Gemperline, *Anal. Chem.* **64**, 599 (1992).
20. J. B. Kruskal, in *Multiway Data Analysis*, R. Coppi and S. Bolasco, Eds. (Elsevier, Amsterdam, 1989), pp. 7–18.
21. R. Tauler, S. Smilde, and B. Kowalski, *J. Chemo.* **9**, 31 (1995).
22. K. Smith, in *Porphyrins and Metalloporphyrins* (Elsevier, Amsterdam, 1975), pp. 871–889.
23. J. E. Falk, in *Porphyrins and Metalloporphyrins* (Elsevier, Amsterdam, 1964), pp. 232–239.
24. M. Gouterman, in *The Porphyrins*, D. Dolphin, Ed. (Academic Press, New York, 1978), Vol. III, pp. 4–11.